Soot Platelets and PAHs with an Odd Number of Unsaturated Carbon Atoms and π Electrons: Theoretical Study of Their Spin Properties and Interaction with Ozone

ARTICLE *in* THE JOURNAL OF PHYSICAL CHEMISTRY A · MARCH 2008

Impact Factor: 2.69 · DOI: 10.1021/jp075487d · Source: PubMed

5 AUTHORS, INCLUDING:

Giovanni Ghigo
Università degli Studi di Torino
54 PUBLICATIONS **1,474** CITATIONS
SEE PROFILE

Glauco Tonachini
Università degli Studi di Torino
96 PUBLICATIONS **1,332** CITATIONS
SEE PROFILE

Soot Platelets and PAHs with an Odd Number of Unsaturated Carbon Atoms and π Electrons: Theoretical Study of Their Spin Properties and Interaction with Ozone

Anna Giordana,[†] Andrea Maranzana,[†,‡] Giovanni Ghigo,[†] Mauro Causà,[*,§] and Glauco Tonachini[*,†]

Dipartimento di Chimica Generale e Chimica Organica, Università di Torino, Corso Massimo D'Azeglio 48, I-10125 Torino, Italy, and Dipartimento di Chimica, Università di Napoli "Federico II", Complesso Universitario di Monte Sant'Angelo, Via Cintia 1, I-80126 Napoli, Italy

Received: July 13, 2007; In Final Form: October 26, 2007

PAHs made from an odd number of unsaturated carbon atoms and π electrons (odd PAHs) have been detected in flames and flank the more familiar even PAHs, having approximately the same quantitative importance, particularly for PAHs containing more than 25 carbon atoms. Similarly, soot platelets containing an odd number of carbon atoms can be reasonably assumed to form during combustion. PAHs are intended here as small models for the investigation of some of their local features. To this end, quantum mechanical calculations were also carried out on periodic models. The spin density patterns were found to be highly dependent on the PAH size and shape. PAHs and soot, once released in the environment, can undergo several oxidation processes. Ozone is then taken as a probe of the reactivity properties of some *internal* exposed portions of a platelet. A primary ozonide (PO) corresponds to an energy minimum, but the relevant concerted addition pathway does not exist, because a PO-like saddle point is second-order. The reaction begins with a nonconcerted attack that produces a trioxyl radical (TR). Subsequent O_2 loss from the TR leaves either an epoxide with a π-delocalized electron or a π-delocalized oxepine, by cleavage of the ring carbon−carbon bond. The initial doublet spin multiplicity thus provides a description of the reaction surface unlike that for the *internal* reactivity of the closed-shell even systems investigated in a previous work, even though the final functionalization is the same.

1. Introduction

Soot aerosol contributes significantly to the atmospheric aerosol mass, given that great quantities of elemental carbon are emitted into the troposphere as a result of biomass and fossil fuel combustion (the estimate is ca. 13 Tg/year). Soot consists of clustered globular particles (whose diameter is ca. 10−80 nm) that are, in turn, made up of irregular and curved graphenic layers or platelets. The particles' structure and composition can vary depending on the source.[1a,2] For instance, both water and salts (namely, ammonium sulfate) can be found associated with carbonaceous aerosol particles. Moreover, the surface is available for interactions with airborne inorganic and organic molecules. Experimental studies on the interaction of soot with small inorganic oxidants, such as NO_2,[3−5] HNO_3,[3] H_2O,[6] and O_3,[6−8] have appeared in the literature.

Polycyclic aromatic hydrocarbons (PAHs) and their derivatives (polycyclic aromatic compounds, PACs) are ubiquitous species, generated from many combustion sources. They are known as primary and secondary tropospheric pollutants. (PAH oxidation can take place both during combustion and at a later time during tropospheric transport.[1]) PAHs and PACs share the same nature of soot,[1,2] because the more or less disordered growing of the graphenic layers takes place in the same combustion processes at low O_2 concentrations that generate the aromatic compounds. Given the origin and structural affinities, PAHs are frequently found in association with carbonaceous particulates.[1b,6,9] In fact, the oxidation of PAHs on soot has been investigated experimentally.[5] PACs have also been supposed to possibly originate on the surface of particulate matter, as they have been detected in diesel exhaust. The oxidation of PAHs and that of soot could share some mechanistic features.

Field investigations and laboratory studies on the functionalization of PAHs[10] have shown that different PAHs decay at different rates during transport. As a consequence, as other products form, the relative amounts of carcinogenic or mutagenic compounds change significantly, and the nature of the secondary pollutants is not known in all cases.[11] Hence, the outcome of gas-phase reactions or heterogeneous processes by which primary pollutants can transform is evidently of chemical and toxicological interest. In particular, functionalization can bring about a polarity increase of the primary pollutants (compounds or particles) and, consequently, of their water solubility. As a result, the aerosol carries them more easily into contact with, for example, the lung tissues. Therefore, PAHs and PACs adsorbed on fine particles are of concern with respect to human health.

Using theoretical tools to study the interaction of ozone with the surface of model soot particles can be helpful in better understanding the results of laboratory studies. The reaction paths studied theoretically are actually relevant to gas-phase reactions, such as those already examined in this laboratory.[12]

* Corresponding authors. E-mail: glauco.tonachini@unito.it (G.T.), mauro.causa@unina.it (M.C.). Fax: ++39-011-2367648 (G.T.), ++39-0181-674202 (M.C.). Web: http://www.thecream.unito.it/(G.T.), http://www.mfn.unipmn.it/∼causa (M.C.).

† Università di Torino.

‡ Present address: Department of Atmospheric, Oceanic, and Space Sciences, University of Michigan, Ann Arbor, MI 48109-2143.

§ Università di Napoli "Federico II".

10.1021/jp075487d CCC: $40.75
Published on Web 01/16/2008

Other groups have worked in recent years on theoretical modeling of soot.[13−18] Unfortunately, structural information about soot and its possibly active surface sites on the atomic scale (which would be useful in setting up a computational study and in calibrating models) is limited. Only a few experimental studies have reported on this issue to some extent.[19]

The present study is preceded by three works on related topics. In the first one,[20] we attempted to define a suitable model for soot and examined the features of the interactions of some small species (H, NO, NO_2, and NO_3) and the gas−solid interaction by which functionalization reactions can take place. In the second work,[21] we addressed the ozonization mechanism for some PAHs containing an even number of unsaturated carbon atoms and π electrons (*even* PAHs), only for nonperipheral positions. In the more recent work,[22] we explored the nature of the oxidized soot surface through a theoretical study of the desorption mechanisms of a variety of polar groups and attempted to contribute to the interpretation of the temperature programmed desorption (TPD) spectra. The present article describes quantum mechanical calculations that were initially carried out on molecular *odd* PAH systems, having an odd number of unsaturated carbon atoms and π electrons, and then extended to periodic systems. PAHs containing an odd number of carbon atoms have been detected in flames and flank the more familiar even PAHs.[23] In a benzene−oxygen flame, the even PAHs are 4−6 times more abundant than the odd PAHs up to ca. 25 C atoms, whereas above 40 C atoms, the concentration difference disappears (see Figure 5 in ref 2). Similarly, soot platelets containing an odd number of carbon atoms can be reasonably assumed to form during combustion. Consequently, our primary goal is to assess the electronic characteristics of these species, particularly their spin density. Then, we can speculate that, as for their even counterparts, once released in the environment, both PAHs and soot platelets can undergo several oxidation processes. PAHs are mainly intended here as suitable small models for the investigation of the local features and reactivity of an *exposed internal portion* of an odd soot platelet. In a soot globular particle, platelets (sharing the same basic structural characteristics as polycylic aromatic hydrocarbons) are superimposed to give the characteristic *turbostratic* structure. The platelets can interact (or even react) with gas-phase molecules, provided that their perimeter or internal positions are not shielded by other more external platelets, as roughly depicted here. To this end, ozone, which

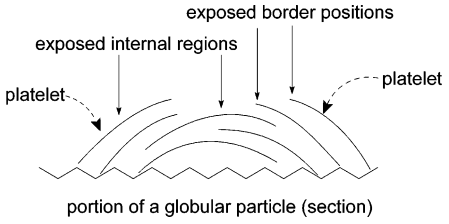

is an important atmospheric oxidant, was used as a probe, and the ozonization mechanism was investigated by the same approach as already adopted for the analogous even systems.[21] Conversely, the reactivity of the peripheral positions for both odd and even systems will be explored and discussed in a forthcoming article.

2. Methods

The stable structures and transition structures (TSs) were determined by gradient procedures,[24] within density functional theory (DFT).[25] The B3LYP functional was chosen, as it is of widespread use and, although prone to underestimate some reaction barriers, has generally performed satisfactorily with respect to geometries and energetics.[26] The polarized 6-31G-(d)[27a] basis set was used in the DFT (B3LYP) optimizations. The nature of the critical points was checked by vibrational analysis (using unscaled vibrational frequencies).[28a,b] For transition structures (TSs), corresponding to first-order saddle points, inspection of the normal mode related to the imaginary frequency was sufficient in most cases to confidently establish their connection with the initial and final stable species, which corresponded to energy minima. In some cases, an IRC calculation[29] helped to confirm the connection with the adjacent energy minima. For the preferred pathway (see below), the energy evaluations were reassessed using the more extended 6-311G(2d,p) basis set[27b] in connection with the 6-31G(d) vibrational analysis.

All molecular calculations were carried out using the Gaussian 03 system of programs.[30]

Periodic LCAO calculations were performed by using the CRYSTAL 2006 program:[31] structures periodic in three (bulk crystals), two (slabs), and one (polymers) dimensions can be treated using Hartree-Fock, density functional [used here, with the B3LYP functional and the 6-21G(d) basis set],[27c] and hybrid Hamiltonians. The periodicity was fully considered by using cyclic boundary conditions: the infinite series of Coulombic integrals were approximated by Ewald techniques,[32] and the infinite exchange series, representing an essentially short-range interaction, were truncated while ensuring convergence of the energy and related observables.[33] The solution of the effective one-electron Schroedinger equations was obtained in reciprocal space,[34] making full use of the space symmetry.[35] All geometries were fully optimized by exploiting analytical gradients.[36] In estimations of the Gibbs free energies, the pressure term $P\Delta V$ was neglected, as is common in condensed phases. Only the partially occupied bands, present only in singlet states, provide contributions to the electronic thermal energy and entropy.[28c]

The spin distribution features were examined by means of the natural population analysis (NPA) approach proposed by Weinhold and co-workers.[37]

For the graphics, the Molden and XCrySDen programs[38] were used.

3. Results and Discussion

Our primary goal, to investigate some of the local features of odd graphenic soot platelets, suggests the use of PAH models. Actual soot platelets could be more extended than the small molecular models adopted in this study. For this reason, the computations were extended to some periodic representations of graphene ribbons that stretch to infinity in one or two dimensions. The periodic computations can thus be seen as another extreme on the size scale. Both are expected to be instrumental in attempting to model a platelet belonging to a soot particle and describe its local chemical features.

3.1. Models. *3.1.1. Molecular Models*. The PAH models chosen have an odd number of carbon and hydrogen atoms and have the same spin multiplicity (doublet) as the periodic models, which have an odd number of electrons per unit cell. They are labeled **M*n***, where ***n*** is the number of carbon atoms.

We examined several models of odd systems (see Chart A in the Supporting Information). They range from the highly symmetric (D_{3h}), almost round ones, through the less symmetric C_{2v} and C_s. The more symmetric ones are **M13**, as an initial D_{3h} nucleus, and its larger homologues **M37**, **M73**, and **M121** (all built from an "**M13** unit" by completely bordering it with hexatomic C rings, one, two, and three times, respectively). **M19**

CHART 1: Odd-PAH Models[a] Employed in This Study: Phenalenyl Radical (M13), Benzo[*cd*]pyrenyl Radical (M19), Dibenzo[*hi,jk*] Ovalenyl Radical (M37), and Esabenzo[*a,bc,d,ef,st,uv*]ovalene (M47)[b]

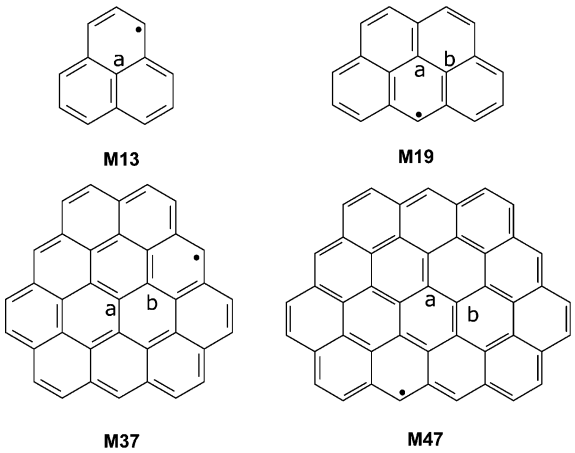

[a] Letters label positions mentioned in the text. [b]Represented by a single resonance structure.

is the simplest representative of a C_{2v} family, built by the same bordering procedure, whose other member are **M47** and **M87**. Other less symmetric model investigated are **M17** (C_s), **M49** (C_{2v}), **M75** (C_s), **M77** (C_s), and **M79** (C_{2v}) (see Chart A in the Supporting Information), all provided with coves of different sizes and shapes. We studied the spin density distribution of all these PAHs and then the reaction mechanism of the attacks of an important oxidant, ozone (at $T = 298$ K), for **M13** and **M19** and, with some limitations, for **M37**, **M47**, and **M49** (Chart 1; the lettering labels some positions that are mentioned in the following discussion).

3.1.2. Periodic Models. We chose four periodic models that resemble the molecular models to some extent. The simplest is **P1**, which has a repeating unit similar to **M13**, with an extra ring as a spacer, introduced to avoid proximity effects. The one-dimensional unit cell consists of a single translational vector, represented by a black arrow (Chart 2). Periodic model **P2** is similar to **P1**, but an additional series of rings is condensed "on top" to provide a wider two-dimensional ribbon (unit cell as above). Periodic model **P3** is again related to **P1**, but it contains a longer spacer, made of three rings. In contrast, model **P4** is periodic in two dimensions. It is reminiscent of the vacancy case studied in our first article,[20] in which a single carbon atom was eliminated from a graphite plane. The vacancy entails having three sp^2 electrons in the plane of the σ system, plus one π electron that is delocalized. However, two of the sp^2 electrons are spin-coupled, and the relevant carbons approach rather close to each. A single σ electron would remain, which in the present model is engaged in binding one hydrogen. We are thus left with just the delocalized π electron, one for each elementary cell. In summary, a hydrogenated carbon vacancy in a 3×3 superlattice of a graphite single layer is defined. These four models were not built along a series as a function of a single parameter. Rather, different extensions were explored in going from **P1** to **P2** and from **P1** to **P3**, whereas **P4** stands alone.

3.2. Spin Density Distribution in the Models. Because the obvious difference between odd and even PAHs lies in the existence of one unpaired electron in the former, the behavior of progressively more extended and delocalized open and closed-shell π systems could be thought of as becoming increasingly alike. To examine this point, the integrated spin density ΔP

CHART 2: Periodic Models P1−P4[a]

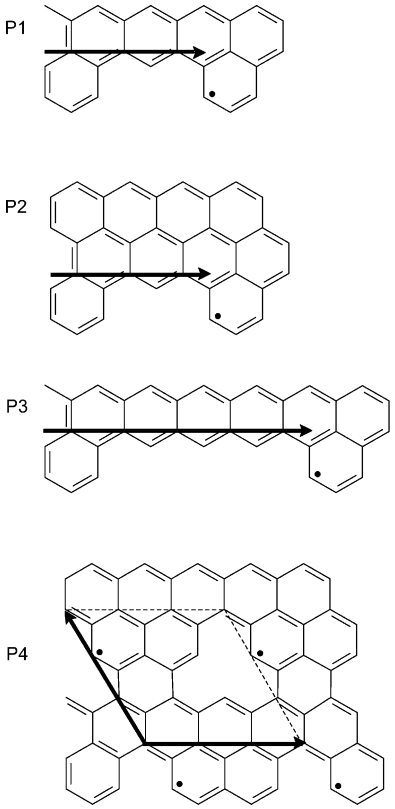

[a] **P1** contains a repeating unit similar to **M13**, with one-ring spacer. The one-dimensional unit cell consists of a single translational vector, represented by a black arrow. **P2** is similar to **P1**, but with a wider two-dimensional ribbon (unit cell as above). **P3** is related again to **P1**, but with a three-ring spacer. **P4**, in contrast, is periodic in two dimensions. It has a hydrogenated carbon vacancy in a 3×3 superlattice of a single graphite layer.

from the NPA ($\Delta P = P^{\alpha} - P^{\beta}$, excess α electron population over β) can conveniently be used. ΔP manifests itself, as expected, as spin waves, i.e., positive spin density values alternating with negative values (which are generally lower in absolute value).[39] This is a common feature of molecular and periodic spin-polarized calculations, because the periodic models (see below) follow the same alternating criteria. By considering increasing size within a homogeneous series (e.g., **M13**, **M37**, **M73**, and **M121**) some trends in the electron density distribution can be observed.

The first feature noticed is that ΔP is rather insensitive to a change in optimized geometry and basis set (as documented by data reported in Chart B, Supporting Information). The second feature is that the spin density is higher on some perimeter positions than on the internal positions, some of which have very low values (Figure 1 illustrates the point for **M37**). Some internal positions, however, have non-negligible spin densities. Third, as the size increases, lower values are found on the perimeter, whereas some internal values can increase. However, the amplitude of the spin waves does not decrease significantly with increasing dimensions of the molecular model or, in the periodic model, of the cell. As a consequence, rather large PAH-like systems with one unpaired electron show several atomic spin density populations with significant values, around 0.2 electrons. On this basis, we can expect that the differences between odd and even systems do not necessarily fade out as the PAHs' size is increased. By further inspecting the ΔP values in the PAHs having a more irregular shape and exhibiting coves, such as **M49** (see also other systems in the Supporting

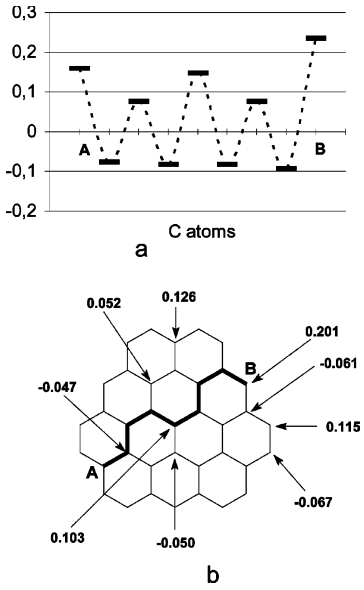

Figure 1. From a DFT(B3LYP)/6-31G(d) calculation: (a) spin waves in the **M37** model shown as the integrated NPA ΔP along the A−B pathway; (b) bold segments indicating the A−B pathway and ΔP numerical values for all internal and perimeter positions. In larger systems, similar patterns were found (see the Supporting Information, Chart B).

Information), one could surmise that less rounded PAHs could generally be more inclined to exhibit rather high ΔP values on internal positions.

Therefore, if the system is attacked by a species sensitive to the ΔP variable, it is reasonable to assume that the attack will be more easily carried out on some perimeter positions rather than internal positions. Yet, we can consider that the number of internal positions increases in the soot platelet approximately quadratically as the system gets larger extending in two dimensions, compared to a quasilinear increase of the perimeter positions. As a consequence, one can expect that the comparison of perimeter vs internal positions becomes more favorable for the latter as the size increases. However, under conditions of elevated concentrations of the attacking species, the functionalization can be expected to proceed beyond the more attractive perimeter positions and to involve many internal sites, particularly if the latter are left uncovered by the outer platelets (see diagram at the end of the Introduction). Because we intended to investigate only the reactivity of *exposed internal positions* of an odd soot platelet in the present phase of our study, we modeled the ozone attack on these positions and compared its features with those discussed in our preceding study on even systems.[21] In a forthcoming extension of this study, we will complete the picture by presenting the comparison between the perimeter reactivities of even- and odd-PAH systems.

An analysis of the electronic structure of the periodic models confirms the features just discussed and, in particular, the stability of the (radical) doublet solutions. A periodic calculation of a model with an odd number of electrons per unit cell allows at least two electronic states.[40] The first state is a closed-shell (metallic) solution, in which the last band is half-full. The second state is a doublet (insulating) solution. The band structures of these two electronic states are depicted in Figure 2 for periodic model **P1**. Because the presence of a closed-shell solution is impossible for an odd-electron *molecular* model, the periodic models provide a further element for discussing the stability of the odd-C π radicals in this case. In all of the periodic models studied here (**P1**−**P4**) the doublet (spin-polarized) state is energetically more stable than the (metallic) closed-shell state: the relative stability of the doublet with respect to the closed shell is −11.1 kcal mol^{-1} for **P1**, −10.2 kcal mol^{-1} for **P2**, −10.0 kcal mol^{-1} for **P3**, and −9.6 kcal mol^{-1} for the **P4** model (in terms of E). Therefore, the spin-polarized electronic structure is ca. 10 kcal mol^{-1} (0.43 eV) more stable than the metallic closed-shell one. Also, when we consider the Gibbs free energy (at $T = 298$ K), the doublet state is more stable than the closed-shell singlet for all the periodic models: −5.5 kcal mol^{-1} for **P1**, −8.6 kcal mol^{-1} for **P2**, −4.4 kcal mol^{-1} for **P3** and −8.7 kcal mol^{-1} for **P4** (see also Table A, p 61, in the Supporting Information). The vibrational contribution was calculated in the harmonic approximation, using unscaled frequencies. For the closed-shell states, the electronic thermal energy and entropy were calculated for the narrow partially occupied band and were found to be below 1 kcal mol^{-1}. In models **P1** and **P3**, the free energy difference departs significantly from the energy difference. In these cases, the structure of the doublet state shows higher vibrational frequencies, which result in a significantly higher vibrational zero-point energy. This, in turn, decreases its relative stability with respect to the closed-shell state, which, however, remains less stable. The present results on periodic models strongly support the conclusion that also in large graphenes, when structural features entail motifs with a local odd number of electrons, the doublet solution is preferred, even if electronic localization allows closed-shell solutions. They also offer a further explanation for why unpaired electrons are commonly found in carbonaceous materials, e.g., in electronic paramagnetic resonance experiments.[41] The reason for the higher stability of the spin-polarized state is evident from the band structure (Figure 2). In the metallic closed-shell (cs) state, the highest, partially occupied band (cut by the Fermi level) is flat and highest in energy: this is a sign of a lower mixing and thus a lesser stability. On the other hand, the band structure of the doublet state (α and β) shows that the highest occupied band, attributed to the α spin states, has a certain bandwidth, a sign of a more extensive mixing and consequently a larger stability. Figure 3 reports isosurfaces of the spin electronic density. Features already observed in the molecular models, such as spin waves and higher spin populations on the border, are present in the periodic models as well.

3.3. Ozone Addition. The possible reaction pathways for ozone addition are sketched in Scheme 1. Having in mind the study of the energy hypersurface corresponding to an overall doublet spin multiplicity ($^1O_3$ + ^{2}PAH), one could wonder whether a quartet surface can be low enough to be involved too. The quartet could be generated in the PAH by promoting one electron from the highest doubly occupied MO to the LUMO (having the SOMO in between). This could be easier in the more extended systems (because the size extension brings about closer MOs). We explored this point to estimate the energy differences for the two states. At the DFT(B3LYP)/6-31G(d) level, for **M13**, the quartet is 108 kcal mol^{-1} above the doublet (using the doublet geometry), which drops to only 93 kcal mol^{-1} if the structure is re-optimized. Going to larger systems, we find 78 kcal mol^{-1} for **M19**, 79 kcal mol^{-1} for **M37**, and 63 kcal mol^{-1} for **M47** (doublet geometries). The trend is approximately as expected, but the energy differences are quite large and rule out any important involvement of the quartet in the ground-state reactivity. Similarly, in the periodic calculations, the following energy differences were found: For the thinner ribbons **P1** and **P3**, values of 74.6 and 66.2 kcal mol^{-1}, respectively, were determined, and for the broader ribbon **P2**, a smaller difference of 46.3 kcal mol^{-1} was calculated. For the

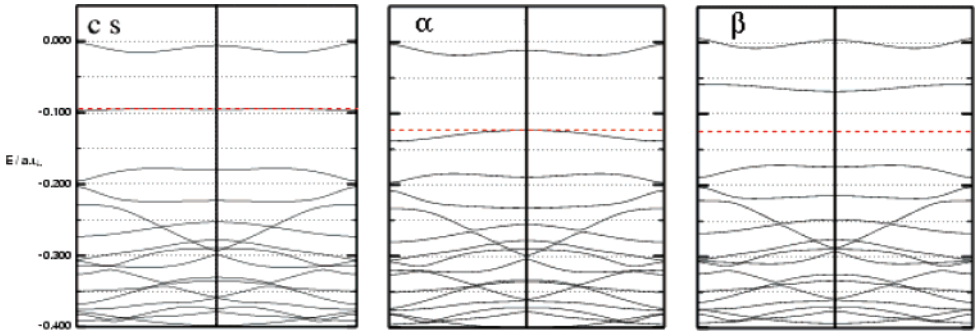

Figure 2. Band structure of periodic model **P1**. The Fermi energy level is represented by the dotted red line. cs, closed-shell metallic state; α and β, spin band structure for the insulating doublet state.

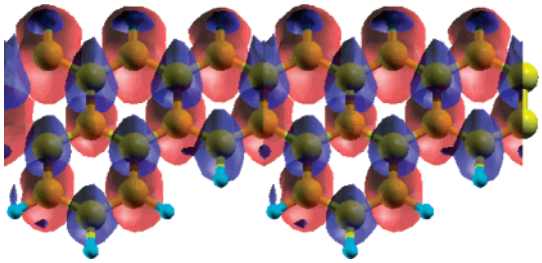

Figure 3. Isosurface of the electronic spin density $[\rho^{\alpha}(\mathbf{r}) - \rho^{\beta}(\mathbf{r})]$. The red isosurface corresponds to +0.001 electrons/bohr^3. The blue isosurface corresponds to −0.001 electrons/bohr^3.

SCHEME 1: Possible Oxidation Pathways (Exemplified for M19)[a]

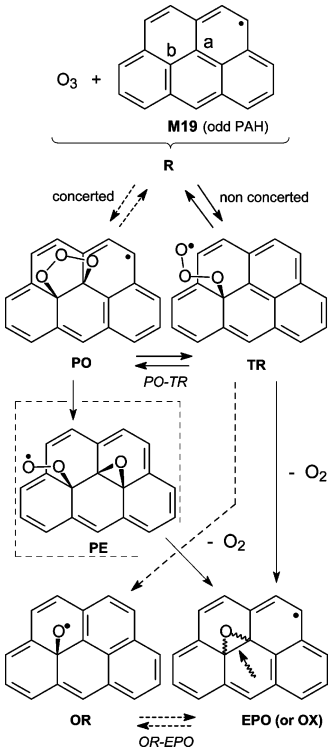

[a] In principle, these lead from the reactants (R) either to the primary ozonide (PO) or to the trioxyl radical (TR). Subsequent bond breakage could then lead, via $^3O_2$ loss, to the final epoxide enantiomers (EPO) or to the isomeric oxepine (OX), through an additional C−C bond breakage (wavy arrow in EPO). The dashed box and dashed arrows indicate intermediate and pathways that were not found.

2D model **P4**, an even smaller but still substantial difference was computed, 22.3 kcal mol^{-1}.

The energetics for the doublet hypersurface are reported in Table 1. As in the preceding articles,[20,21] acronyms are used to label intermediates and transition structures that connect them. The addition to the unsaturated system can, in principle, take place either by a concerted process (in which the two C−O bonds form in a more or less synchronous way) or by a two-step process. Whereas a concerted attack would directly lead to the primary ozonide intermediate (PO, with a local 1,2,3-trioxolane structure), the two-step pathway first produces an open-chain trioxyl radical (TR). Some evident differences between an odd PAH and an even PAH[21] can be noted right from the beginning. For an even PAH, the initial PO is a closed-shell molecule; for an odd PAH, the π-delocalized PO is instead a π radical (which we could call "π·PO"), because it obviously maintains an odd number of π electrons. On the other hand, for an odd PAH, TR is a rather localized O radical with a closed-shell π system on the PAH part. By contrast, the nonconcerted addition of O_3 to an even PAH produces a diradical. These traits are also present in the odd-PAH product (π·EPO) and in the odd-PAH oxyl intermediate (OR) shown in Scheme 1. Other intermediates can be imagined, such as an oxyl peroxyl species (OP) formed by O−O bond breaking in PO (which, however, is a high-energy triradical) or a peroxyl epoxide (PE), coming from epoxide ring closure in OP. The latter intermediate was found only for **M13** and involved a perimeter position. In the other models, a PE intermediate does not exist because dioxygen dissociates spontaneously from the rest of the molecule, leaving the epoxide.

3.3.1. Primary Ozonides. The primary ozonide is usually considered to be the first intermediate in the attack of ozone on an unsaturated system.[42] It can first be observed that different attacks are conceivable. Although the **M13** model (Chart 1) allows an attack that involves the central carbon (position a), in which ozone would add 1,2 to two tertiary carbons, the resulting π·PO could not be classified as a completely internal addition, because one of the C atoms involved lies on the molecular perimeter. The two larger systems, **M19** and **M37**, instead allow O_3 attacks on purely internal positions (a and b). Only the most stable adducts will be discussed in the following subsections. All π·POs were found as energy minima. The step was found to become less endoergic as the system moves from **M13** and **M19** (13.4−13.5 kcal mol^{-1}) to the more extended **M37** (10.8 kcal mol^{-1}). Part of the energy cost can be attributed to the pyramidization and change in hybridation of the attacked carbons. (As the system extends, part of the strain can be distributed to a limited extent over a larger series of bonds and angles.) The deformation energies can be assessed by single-point energy computations on the PO structures devoid of the O−O−O moiety. They are 59.2 (**M13**), 56.3 (**M19**), and 55.3 (**M37**) kcal mol^{-1}.

3.3.2. Search for a Concerted Addition Step Leading to the π·PO. Having assessed the existence, on the energy hypersur-

TABLE 1: Energies, Enthalpies, and Free Energies[a] of the Initial Transition Structures and the Stablest Intermediates

	substrate[b]									
	M13			**M19**			**M37**			**M47**
structure[c]	ΔE	ΔH	ΔG	ΔE	ΔH	ΔG	ΔE	ΔH	ΔG	ΔE
PO	13.4	14.2	27.9	13.5	14.5	28.6	10.8	12.8	26.2	
R−TR TS	17.7	17.6	29.9	8.1	8.9	21.1	1.9	3.4	14.4	5.4
TR	16.3	17.7	29.1	3.9	5.7	16.9	−3.7	−1.3	9.3	1.2
TR−PO TS	25.6	24.5	37.7	22.1	22.1	36.1	−	−	−	
$^3O_2$ loss TS	16.6[d]	16.2[d]	27.3[d]	4.4[e]	5.4[e]	16.6[e]	−3.1[e]	−1.5[e]	9.0[e]	1.6
EPO + $^3O_2$	−14.8[f]	−	−	−16.7	−17.7	−15.3	−18.0	−17.5	−16.6	−18.9
EPO−OX + $^3O_2$ TS	−	−	−	−16.4	−17.4	−15.0	−11.5	−12.0	−10.7	
OX + $^3O_2$	−27.8	−27.7	−26.0	−23.5	−23.3	−21.4	−13.3	−12.9	−11.9	−11.8

[a] Relative to the reactants R; in units of kcal mol^{-1} (T = 298.15 K). [b] See Chart 1 (for **M47**, the vibrational analysis could not be carried out). [c] For structure labels, see Scheme 1. [d] TS leading to OX. [e] TS leading to EPO. [f] Spontaneously undergoes ring expansion to oxepine (OX); this is an estimate of the energy of an epoxidic structure obtained by constrained optimization (C−C bond frozen).

SCHEME 2: Concerted O_3 Attacks on (a) the Dibenzoindenyl Radical, a System That Contains a Symmetry Plane (τ, Dashed Line), to Allow the Easier Detection of Second-Order Saddle Points,[a] and (b) M19

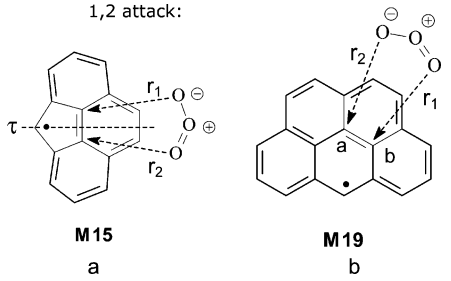

[a] See text.

face, of more or less stable primary ozonides, it is necessary to determine whether these intermediates can be directly reached from the reactants via a concerted transition structure. This kind of attack is not expected to take place in a perfectly synchronous manner, because of the lack of symmetry. Searches for an R−PO TS corresponding to a concerted addition were unsuccessful. Our attempts hinted instead at the possible presence of second-order saddle points (maxima along two geometrical directions). To further verify that a concerted attack cannot correspond to a first-order saddle point (corresponding to a TS), a more symmetric attack was studied on another odd-C model, **M15**, the dibenzo homologue of the indenyl radical (Scheme 2a).

This model provided the indication that the concerted attack that could, in principle, directly produce a PO does indeed correspond to a second-order saddle point on the energy hypersurface (**II** in Figure 4). The two imaginary frequencies (Scheme 3) are related to normal modes that connect structure **II** either (i) to the reactant moieties and to the ozonide (the direction from reactants through **II** to PO in Figure 4; symmetric stretching in Scheme 3) or (ii) to the first step of the nonconcerted pathway, which proceeds through trioxyl radical (TR) intermediates (the direction from TR through **II** to TR in Figure 4; antisymmetric stretching in Scheme 3). The **II** saddle point corresponds to C−O distances of 1.949 Å.

To characterize the situation for an asymmetric case as well, we undertook the (rather burdensome) task of drawing a 2D map for **M19**, by way of a series of constrained optimizations corresponding to selected values of r_1 and r_2 (Scheme 2b). For each pair of values (held frozen), the remaining parameters were fully optimized. The thus-obtained map (Supporting Information, Figure A) reflects the asymmetric situation present in **M19**. In fact, whereas the nonconcerted attack to position b, related to a shortening of r_1, leads to a relatively stable trioxyl radical intermediate (4 kcal mol^{-1} above the reactants), the nonconcerted attack to position a, corresponding to a shortening of r_2, leads to an intermediate that is 18 kcal mol^{-1} above the reactants. Consistently, the second-order saddle point that separates the two nonconcerted reaction pathways, and would correspond to a hypothetical concerted (but asynchronous, in this case) attack, was not found along the bisector of the map ($r_1 + r_2$ direction). As in Figure 4, it can be seen as separating the two zones of the TR−PO transition structures or the reactants from PO (imaginary vibrational frequencies for the antisymmetric and symmetric C−O stretches). Therefore, Figure 4 qualitatively also depicts the situation that can be found when dealing with asymmetric cases, but to a certain extent, because the upper left part and lower right part are no longer equivalent.

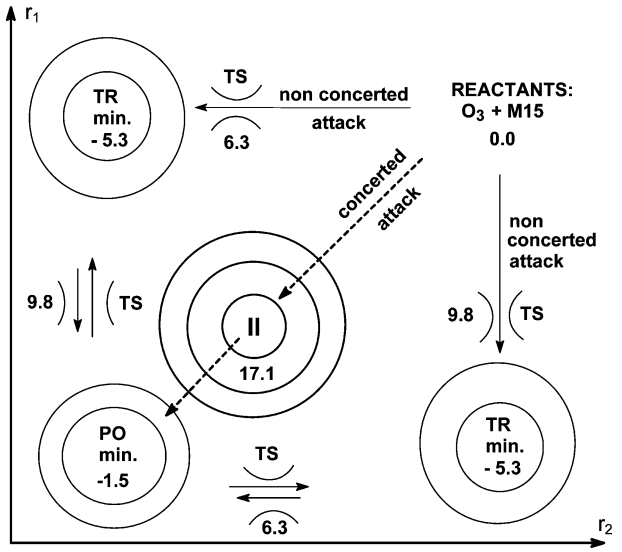

Figure 4. Qualitative topology of the energy surface (E) for **M15**, corresponding to the concerted attack (dashed arrows), which does not correspond to a reaction pathway, and the equivalent nonconcerted reaction pathways that go through trioxyl radicals (TRs). Along the dashed arrow, the energy goes up from reactants to **II**, the second-order saddle point, and then down again to PO. Energy differences are in kcal mol^{-1}.

SCHEME 3

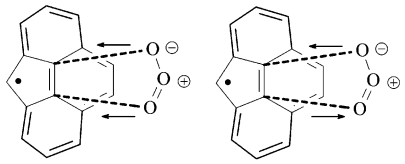

TABLE 2: 6-311G(2d,p) Energies and Estimates of the Free Energies[a] for the Preferred Pathway

	substrate[b]		
structure[c]	**M13**	**M19**	**M37**
PO	15.0 (29.4)	15.3 (30.4)	12.7 (28.1)
R−TR TS	**18.0** 18.2 (**30.3** 30.5)	**8.4** 8.4 (**21.4** 21.4)	2.1 (14.6)
TR	**16.6** 16.6 (**29.3** 29.3)	**4.4** 4.4 (**17.5** 17.5)	−2.6 (10.3)
TS for O_2 loss	17.0 (27.6)[d]	4.7 (16.9)[e]	−2.3 (9.9)[e]
EPO + O_2	−	−16.1 (−14.7)	−17.4 (−15.9)
OX + O_2	−28.2 (−26.6)	−23.9 (−21.8)	−13.8 (−12.5)

[a] Relative to the reactants; all values in kcal mol^{-1}. The estimates of the free energies (in parentheses) were obtained by combining the 6-31G(d) data from the vibrational analysis with the 6-311G(2d,p) energies. Bold data refer to structures that were fully optimized with the larger basis set. They are quite close to the values (lightface) obtained by single-point *E* computations on the 6-31G(d) geometries. [b] See Chart 1. [c] For labels, see Scheme 1. Transition structures are identified by the labels of the minima they connect. [d] Leading to OX. [e] Leading to EPO.

Finding a second-order saddle point contrasts our previous findings for the even systems, for which a PO-like TS exists (although it is unfavored with respect to the TS for the nonconcerted attack; see below).

3.3.3. Trioxyl Radicals. Upon nonconcerted ozone attack on the PAH, only one C−O bond forms in the first step, and a trioxyl radical TR results. All systems allow this kind of O_3 attack on a purely internal position. The most internal position a (Chart 1) was chosen for **M13** and **M37**; for **M19** and **M47**, position b was chosen instead, because the attack at position a results in a triradical. (As tested for **M19**, the attack at position a implies $\Delta E = 18.9$ and $\Delta E^{\ddagger} = 19.8$ kcal mol^{-1}.) The TR intermediates form with variable effort. For the smaller ones, **M13** and **M19**, they are higher in energy than the reactants by 16 and 4 kcal mol^{-1}, respectively. For **M37**, by contrast, the step is exoergic by −4 kcal mol^{-1}. A further extension of the model brings about, unexpectedly, an almost-isoergic step (+1 kcal mol^{-1}). As for the PO intermediates, this can, in part, be attributed to the deformation undergone by the hydrocarbon framework. However, the absolute values of the deformation energies are significantly smaller: 34, 32, 27, and 28 kcal mol^{-1} (to be compared with the PO values, which are all larger than 55 kcal mol^{-1}). This first step (which occurs along the preferred pathway) was, in fact, studied with two basis sets: 6-31G(d) and 6-311G(2d,p) (see Table 2). The estimates of the free energies (in parentheses) were obtained by combining the data from the 6-31G(d) vibrational analysis with the 6-311G(2d,p) energies. The energy and free energy differences included in the following discussion are those obtained with the 6-311G-(2d,p) basis set. The step from reactants to TR is endoergic for **M13** by 17 kcal mol^{-1} in terms of *E*, which becomes 25 kcal mol^{-1} for the *G* estimate. For **M13**, the ΔE barrier between the reactants R and TR is 18 kcal mol^{-1}, or almost 25 kcal mol^{-1} in terms of *G*.

In the case of **M19**, the step is more favorable (significantly less endoergic). TR is some 4 kcal mol^{-1} with respect to R in terms of *E*, or 17 kcal mol^{-1} in terms of *G*. This corresponds to lower barriers, 8 and <21 kcal mol^{-1}, for *E* and *G*, respectively. It is clear (compare bold versus lightface values in Table 2) that fully optimizing the TS (R−TR) and TR structures for **M13** and **M19** with the more extended basis set leads to insignificant changes in the energy differences (at most 0.2 kcal mol^{-1}) with respect to the single-point 6-311G (2d,p)//6-31G(d) energy computations. Therefore, for the critical points that follow, we limited our calculations to the 6-311G (2d,p)//6-31G(d) energy evaluation. Extending the system to **M37** results in an even easier attack. The energy change from R to TR drops to −3 kcal mol^{-1}. In this case, the barrier with respect to the separate reactants goes down to 2 kcal mol^{-1} in terms of *E* and to 15 kcal mol^{-1} in terms of *G*. A clear trend can be observed: the reaction step is described as slightly more difficult when the more extended basis set is used, and the corrections due to improvement of the basis set vary very little in going from one system to another. In fact, both the step ergicity and barrier height are affected in a regular way, by ca. 1 kcal mol^{-1}.

In summary, the trioxyl radicals are the only intermediates that can form directly from the reactants, and the formation energy barrier can be assumed to vary with the size of the PAH. We extended the study to the **M47** model, for which, however, we obtained only 6-31G(d)//6-31G(d) energy results. Although the model is larger, its spin density on the attacked internal position is slightly lower than that attacked in **M37**.

A qualitative inverse correlation (Figure B in the Supporting Information) between the barrier heights and the rising spin density values at the internal positions attacked was found ($\Delta E^{\ddagger} = 18$, 8, 5, and 2 kcal mol^{-1} vs $\Delta P = 0.07$, 0.09, 0.10, and 0.15 e for **M13**, **M19**, **M47**, and **M37**, respectively). Yet, the trend cannot be plainly attributed to the size parameter only.

The addition of dioxygen, in competition with ozone, to an internal position of an odd platelet, just after its formation, could destroy its characteristics. The platelet would become an even π system decorated by a peroxyl radical group. To assess whether this reaction can be competitive, we studied the **M13**, **M19**, and **M37** + O_2 radical couplings. Even though the involved central positions in these systems has, as seen, non-negligible spin densities, no peroxyl intermediates could be found, because the interaction is repulsive (see Figure C in the Supporting Information).

3.3.4. Trioxyl Diradical to Primary Ozonide Interconversion. The π·PO adduct could have a role only if its energy minimum could be reached from the minimum of the initial adduct TR. Therefore, to complete the picture of these initial steps, the TR $\rightleftarrows$ PO interconversion was investigated. A barrier of 9.3 kcal mol^{-1} is present for **M13** in terms of *E* (12.2 kcal mol^{-1} for the reverse process). In terms of *G*, these barriers are estimated to be 8.6 and 9.8 kcal mol^{-1}, respectively (Table 1). In the case of **M19**, the TR−PO energy barrier becomes 18.2 kcal mol^{-1} (19.2 kcal mol^{-1} in terms of *G*). In view of the very unfavorable competition with the loss of dioxygen from TR (see the next subsection), this investigation was not extended to the case of **M37**. In sharp contrast is the case of the even PAHs: a thorough search for an interconversion TS gave the result that this process cannot take place directly,[21] and PO and TCD (the trioxylcyclohexadienyl diradical, equivalent to TR) were shown to possibly interconvert only by dissociating back to the reactants R.

3.3.5. From the Trioxyl Radicals to the Epoxides or Oxepines. Upon dioxygen loss, formation of an oxyl radical would be conceivable if closure of the epoxide ring were not spontaneous (Scheme 1). The oxyl radical (OR) can be found as a critical point for **M13** and **M37** upon symmetry-constrained optimization (ternary symmetry). However, it is not an energy minimum,

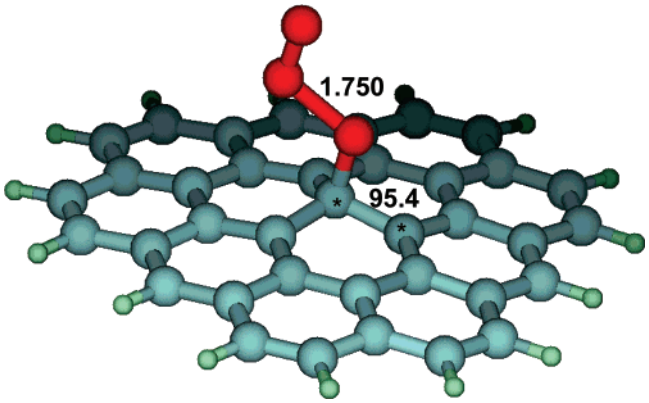

Figure 5. TR−EPO TS for **M37**. O−O bond length in Å, ∠OCC (starred carbons) in degrees.

but a higher-order saddle point. Consequently, if the constraint is removed, the structure collapses to the epoxide or to the relevant oxepine spontaneously. For **M19**, OR cannot be found at all. In **M13**, TR directly gives an oxepine, because the would-be epoxidic C−C bond breaks spontaneously. An estimate of the energy of a hypothetical epoxide can be obtained by forcing this bond not to cleave while optimizing the remaining geometrical parameters (Table 1, value in italics). TR in **M19** gives, upon dioxygen loss, either an epoxide or, preferentially, an oxepine. The reverse is true for the more rigid **M37** and **M47** systems, in which the epoxide ring encounters some difficulty in opening to give the oxepine (Figure 6). Also, for **M49**, the epoxide is located at −15.4 kcal mol^{-1} with respect to the separate reactants, whereas the oxepine is at −13.5 kcal mol^{-1}.

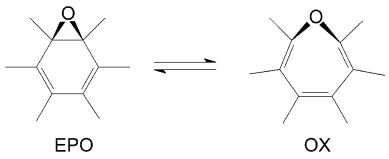

Regarding the main geometric features of the O_2-loss transition structures (Figure 5), one can notice that the main changes that take place in a concerted manner are not synchronous. The breaking O−O bond is stretched to some extent: +10% for **M13** (1.721 vs 1.560 Å in TR), +9% for **M19** (1.750 vs 1.601 Å in TR), +13% for **M37** (1.750 vs 1.549 Å in TR), and +9% for **M47** (1.740 vs 1.600 Å in TR). By contrast, the OCC angle that is closing upon formation of the epoxide ring is still rather open. The TS values can be compared, on one hand, with the initial values in TR and, on the other hand, with the final values. The ∠OCC values in TR are 97.3° (**M13**), 97.4° (**M19**), 96.7° (**M37**), and 96.6° (**M47**). For **M13**, the ∠OCC value in the final oxepine is 38.7°, whereas in the two final epoxides, the values are 56.6° (**M19**), 59.0° (**M37**), and 58.7° (**M47**). The values in the TS are 95.2° (**M13**), 96.0° (**M19**), 95.4° (**M37**), 95.2° (**M47**) and correspond to a degree of ring closure of ca. 3.5%. A final comment on the O_2-loss transition structures concerns the role of OR: the geometrical features of these structures, in which the oxygen bound to carbon is slightly bent on one side, suggest that OR (for **M13** and **M37**) is likely to simply be bypassed.

3.3.6. Periodic Calculations. The internal positions attacked by ozone in the periodic models show spin density values close to 0.1. The energy differences relevant for the formation of the TR species in the **P*n*** models are reported in Table 3. It can be noted that, in the case of **P4**, no trioxyl derivative is found (the interaction is plainly repulsive). These models differ in such a way (wider band for **P2** compared to **P1**; larger spacer for **P3** compared to **P1**; **P4** is the only bidimensional model) that we cannot expect to observe regular trends. In the molecular models, some lowering of the step energy occurred in going from **M13** to **M37** (from 16 to −4 kcal mol^{-1}) and, to a lesser extent, from **M19** to **M47** (from 4 to 1 kcal mol^{-1}). Here, the periodic model more closely related to one of the molecular models is **P3**, in which an **M13**-like unit is repeated with a sufficiently large spacer to avoid proximity effects. In this case, a step energy of 10 kcal mol^{-1} was found, which could be compared with the **M13** value, 16 kcal mol^{-1}. By comparing the molecular (**M13**) and periodic (**M13**-like) models, we can tentatively attribute the larger stability of the latter to the fact that it appears to be more easily curved along the direction indicated by the arrow in Chart 2. (This aspect will be investigated in future work.) The relevant deformation energies are 25.5, 24.9, and 27.2 kcal mol^{-1}, obtained by removing the oxygen atoms to leave the hydrocarbon frameworks **P1**−**P3**. These values appear to be closer to those computed for the two larger molecular models (27−28 kcal mol^{-1}) than for the two smaller models (34−32 kcal mol^{-1}).

TABLE 3: Periodic Calculations: Energy Differences[a]

	substrate[b]			
structure[c]	**P1**	**P2**	**P3**	**P4**
TR	−1.8 (25.5)	−9.1 (24.9)	−10.3 (27.2)	−
EPO + O_2	−	−	−13.0[d]	−40.7
OX + O_2	−48.8	−41.7	−51.6	−

[a] Relative to ozone + the periodic hydrocarbon model **P*n***; deformation energies within parentheses; values in kcal mol^{-1}. [b] See Chart 1. [c] For structure labels, see Scheme 1. [d] Spontaneously undergoes ring expansion to oxepine (OX); this is an estimate of the energy of an epoxidic structure obtained by constrained optimization (C−C bond frozen).

Upon dioxygen loss, the periodic models yield an oxepine (**P1**, **P2**, and **P3**) or an epoxide (**P4**). The ring enlargement is evidently easier in the first three systems, in which the C−C bond cleavage is even spontaneous. For the bidimensional model, the formation of a seven-membered ring is impossible, and an epoxide is obtained instead, with a gain of −41 kcal mol^{-1}. The energies involved (42−52 kcal mol^{-1}) are significantly larger than those related to oxepine formation in the **M*n*** models, which decrease as the system gets larger and stiffer: −28, −23, −13, and −12 kcal mol^{-1} for **M13**, **M19**, **M37**, and **M47**, respectively. The largest values are found for the more flexible **P1** and **P3** models (thin ribbon), whereas **P2**, with its wider band, exhibits a slightly more moderate stabilization (by 7−10 kcal mol^{-1}). For **P3**, a constrained optimization (in which the C−C bond cleavage is not permitted) yields an epoxidic structure with an energy gain of −13 kcal mol^{-1}. This can be compared with the almost −15 kcal mol^{-1} value obtained by a similar procedure for **M13**, in which the C−C bond would also cleave spontaneously. Again, we can tentatively offer an explanation for the larger stability of the oxepine derived from **P3** with respect to that coming from **M13**. The periodic model more easily acquires a more pronounced curvature along the ribbon direction than the molecular model. This can be demonstrated by some deformation energy computations. The first datum is the deformation energy required for the parent **M13** to be as curved as its oxepine derivative, 90 kcal mol^{-1}. For **P3**, 98 kcal mol^{-1} is necessary for the structure to become as curved as its oxepinic derivative (larger curvature). To be as curved, **M13** would necessitate 121 kcal mol^{-1}. This verifies the greater flexibility of the periodic model.

In considering the reaction of O_3 with a model of soot platelet and the comparison of the molecular and periodic models, we can draw attention to some common aspects. We could also recall the experimental work of Schurath, Saathoff, and co-workers[8] on the soot−ozone interaction. We referred to that investigation in our preceding study on the ozonization of internal positions of even PAHs. Also, in the present case, the theoretical study of both kinds of models confirms that the functionalization of the soot surface corresponds to the formation of epoxidic groups, with dioxygen loss and regeneration of the π-delocalized system. If some structural flexibility is locally present, it can allow for some cleavage of C−C bonds internal to epoxidic rings, thus forming oxepinic structures.

4. Conclusions

Polycyclic aromatic hydrocarbons containing an odd number of carbon atoms (odd PAHs) have been detected in flames and have approximately the same quantitative importance of the more familiar even PAHs, particularly if the number of carbon atoms is greater than 25. This article focused on the features and reactivity of these π radicals, seen also as models for odd soot platelets. Periodic model systems related to the odd PAHs were also exploited to address the same issues. Both molecular and periodic simulations of the oxidation processes of these substrates were limited here to internal positions only, with the purpose of modeling *exposed internal portions* of odd soot platelets. This study considered (i) their spin density distributions and (ii) the oxidative functionalization that odd PAHs can undergo as a consequence of ozone electrophilic attack.

Spin Density. ΔP is higher on some perimeter positions than on most internal positions. However, some internal positions have non-negligible spin densities, and the number of internal positions increases in the soot platelet approximately quadratically as the system grows, whereas the number of the perimeter positions undergoes a quasilinear increase. One can thus expect that the comparison of perimeter vs internal positions becomes more favorable for the latter as the size increases. Indeed (i) upon size extension, lower values are found on the perimeter, whereas some internal values increase, and (ii) PAHs having a more irregular shape and exhibiting coves generally seem to exhibit rather high ΔP values on internal positions. If the system is attacked by a species sensitive to the spin density property, it is reasonable to assume that the attack will be more easily carried out on some perimeter positions rather than internal positions. However, under conditions of elevated concentrations of the attacking species, the functionalization can be expected to go beyond the more attractive perimeter positions and involve many internal sites. Also, the differences between odd and even systems are not expected to fade out as the PAH becomes larger, because the amplitude of spin waves does not decline with the increasing dimensions of the molecular model or, in the periodic model, of the cell.

Ozonization Pathways. Although some different possible reaction pathways were considered, only the primary ozonide (π•PO) and the trioxyl radical (TR) were found to intervene as rather stable intermediates. Moreover, of these, only the latter (more stable in the two more extended models) was found to be representative of an oxidation reaction pathway connecting the reactants R (PAH + O_3) and the final products. This is because PO cannot form directly from R, and the nonconcerted step leading to TR is the only one through which the system can pass. (By contrast, in the even systems, a PO-like transition structure could be found.) In addition, the PO formation step from TR (although an interconversion TS was found, at variance with the results for even systems) cannot compete with the O_2 loss step that transforms TR into an epoxide (EPO) or an oxepine (OX) by further C−C bond cleavage. O_2 loss from TR can also, in principle, give an oxyl diradical (OR), but this intermediate does not exist in one case and is rather high in energy in the other two cases, in which it seems to be bypassed by the reacting system. In one case, OX forms directly, and in the other two, EPO can undergo ring opening to it, but in one case, OX is to some extent less stable. In conclusion, ozonization of internal positions of an odd system has to pass through the trioxyl radical intermediate to finally produce an epoxide or the related oxepine. This is the same outcome as found for the even systems. The energetics of the preferred reaction pathways are summarized in Figure 6.

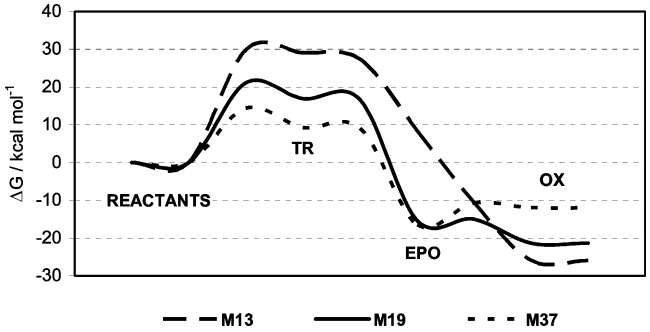

Figure 6. Free energy profiles for the preferred reaction pathways going through internal trioxyl radicals to epoxides and oxepines. The TSs between TR and PO lie at higher free energies than the TR−EPO TS.

Acknowledgment. Financial support from the Italian MIUR is gratefully acknowledged [PRIN-COFIN 2004, "Studio integrato sul territorio nazionale per la caratterizzazione ed il controllo di inquinanti atmosferici (SITECOS)"]. A generous grant provided by Regione Piemonte is also acknowledged (DD n.1 18.1.2006, DD n. 64 2.12.2005, Bando Ricerca Scientifica - Settore Sviluppo Sostenibile). This work was conducted within the framework of EC FP6 NoE ACCENT (Atmospheric Composition Change, the European NeTwork of Excellence). A.G. (Ph.D. student, Dottorato di Ricerca in Scienze Chimiche, XX ciclo) is supported by a grant provided by the Regione Piemonte.

Supporting Information Available: Geometries of all optimized structures, corresponding total energies, and some information about atomic spin densities. This material is available free of charge via the Internet at http://pubs.acs.org.

References and Notes

(1) (a) Finlayson-Pitts, B. J.; Pitts, J. N., Jr. *Chemistry of the Upper and Lower Atmosphere*; Academic Press: New York, 2000; Chapter 10, Sections E and F. (b) Finlayson-Pitts, B. J.; Pitts, J. N., Jr. *Chemistry of the Upper and Lower Atmosphere*; Academic Press: New York, 2000; Chapter 10, section A, §4.

(2) Homann, K.-H. *Angew. Chem., Int. Ed.* **1998**, *37*, 2434−2451.

(3) Kirchner, U.; Scheer, V.; Vogt, R. *J. Phys. Chem. A* **2000**, *104*, 8908−8915.

(4) Arens, F.; Gutzwiller, L.; Baltensperger, U.; Gäggeler, H. W.; Amman, M. *Environ. Sci. Technol.* **2001**, *35*, 2191−2199.

(5) Lu're, B. A.; Mikhno, A. V. *Kinet. Catal.* **1997**, *38*, 490−497.

(6) Pöschl, U.; Letzel, T.; Schauer, C.; Niessner, R. *J. Phys. Chem. A* **2001**, *105*, 4029−4041. Schauer, C.; Niessner, R.; Pöschl, U. In *Transport and Chemical Transformation of Pollutants in the Troposphere, Proceedings from the EUROTRAC-2 Symposium 2002*, p 273, poster CMD-44; Midgley, P. M., Reuther, M., Eds.; Backhuys Publishers: Leiden, The Netherlands; Margraf Verlag: Weikersheim, Germany, 2002; CD-ROM ISBN 3-8236-1385-5; *Environ. Sci. Technol.* **2003**, *37*, 2861.

(7) Fendel, W.; Matter, D.; Burtscher, H.; Schmidt-Ott, A. *Atmos. Environ.* **1995**, *29*, 967−973.

(8) Kamm, S.; Mohler, O.; Naumann, K.-H.; Saathoff, H.; Schurath, U. *Atmos. Environ.* **1999**, *33*, 4651−4661.

(9) Kamens, R. M.; Guo, J.; Guo, Z.; McDow, S. R. *Atmos. Environ.* **1990**, *24A*, 1161−1173.

(10) Atkinson, R.; Arey, J. *Environ. Health Perspect.* **1994**, *102* (Suppl. 4), 117−126.

(11) Pitts, J. N., Jr.; Lokensgard, D. M.; Ripley, P. S. van Cauwenberghe, K. A.; van Vaeck, L.; Schaffer, S. D.; Thill, A. J.; Belser, W. L. *Science* **1980**, *210*, 1347−1349.

(12) Ghigo, G.; Tonachini, G. *J. Am. Chem. Soc.* **1998**, *120*, 6753−6757. Ghigo, G.; Tonachini, G. *J. Am. Chem. Soc.* **1999**, *121*, 8366−8372. Ghigo, G.; Tonachini, G. *J. Chem. Phys.* **1999**, *109*, 7298−7304. Motta, F.; G. Ghigo, G.; Tonachini, G. *J. Phys. Chem. A* **2002**, *106*, 4411−4422. Ghigo, G.; Maranzana, A.; Causà, M.; Tonachini, G. *J. Phys. Chem. A* **2006**, *110*, 13270−13282.

(13) (a) Montoya, A.; Truong, T.-T. T.; Mondragón, F.; Truong, T. N. *J. Phys. Chem A* **2001**, *105*, 6757−6764. (b) Montoya, A.; Mondragón, F.; Truong, T. N. *J. Phys. Chem A* **2002**, *106*, 4236−4239. (c) Montoya, A.; Mondragón, F.; Truong, T. N. *Carbon* **2003**, *41*, 29−39. (d) Espinal, J. F.; Montoya, A.; Mondragón, F.; Truong, T. N. *J. Phys. Chem B* **2004**, *108*, 1003−1008.

(14) Frankcombe, T. J.; Smith, S. C. *Carbon* **2004**, *42*, 2921−2928.

(15) Sendt, K.; Haynes, B. S. *J. Phys. Chem. A* **2005**, *109*, 3438−3447.

(16) Radovic, L. R.; Bockrath, B. *J. Am. Chem. Soc.* **2005**, *127*, 5917−5927.

(17) Chen, N.; Yang, R. T. *Carbon* **1998**, *36*, 1061−1070.

(18) Kiotani, T.; Tomita, A. *J. Phys. Chem. B* **1999**, *103*, 3434−3441.

(19) Petzold, A.; Stein, C.; Nyeki, S.; Gysel, M.; Weingartner, E.; Baltensperger, U.; Giebl, H.; Hitzenberger, R.; Dopelheuer, A.; Vrchoticky, S.; Puxbaum, H.; Johnson, M.; Hurley, C. D.; Marsh, R.; Wilson, C. W.; *Geophys. Res. Lett.* **2002**, *30*, 1719−1722. Grothe, H.; Muckenhuber, H. In *The Third Informal Conference on Reaction Kinetics and Atmospheric Chemistry*; Copenhagen Center for Atmospheric Research: Copenhagen, Denmark, 2002. Blake, D. F.; Kato, K. *J. Geophys. Res.* **1995**, *100*, 7195−7202. Peuschl, R. F.; Boering, K. A.; Verma, S.; Howard, S. D.; Ferry, G. V.; Goodman, J.; Allen, D. A.; Hamill, P. *J. Geophys. Res.* **1997**, *102*, 13113−13118. Harris, P. J. F. *Crit. Rev. Solid State Mater. Sci.* **2005**, *30*, 235−253. Muckenhuber, H.; Grothe, H.; *Carbon* **2007**, *45*, 321−329. Sadezky, A.; Muckenhuber H.; Grothe, H.; Niessner, R.; Poschl, U. *Carbon* **2005**, *43*, 1731−1742. Kamm, S.; Saathoff, H.; Naumann, K. H.; Mohler, O.; Schurath, U. *Combust. Flame* **2004**, *138*, 353−361 and references therein.

(20) Ghigo, G.; Maranzana, A.; Tonachini, G.; Zicovich-Wilson, C. M.; Causà, M. *J. Phys. Chem. B* **2004**, *108*, 3215−3223.

(21) Maranzana, A.; Serra, G.; Giordana, A.; Tonachini, G.; Barco, G.; Causà, M. *J. Phys. Chem. A* **2005**, *109*, 10929−10939.

(22) Barco, G.; Maranzana, A.; Ghigo, G.; Causà, M.; Tonachini, G. *J. Chem. Phys.* **2006**, *125*, 194706.

(23) Keller, A.; Kovacs, R.; Homann, K.-H. *Phys. Chem. Chem. Phys.* **2000**, *2*, 1667−1675.

(24) Pople, J. A.; Gill, P. M. W.; Johnson, B. G. *Chem. Phys. Lett.* **1992**, *199*, 557−560. Schlegel, H. B. In *Computational Theoretical Organic Chemistry*; Csizsmadia, I. G.; Daudel, Eds.; Reidel Publishing Co.: Dordrecht, The Netherlands, 1981; pp 129−159. Schlegel, H. B. *J. Chem. Phys.* **1982**, *77*, 3676−3681. Schlegel, H. B.; Binkley, J. S.; Pople, J. A. *J. Chem. Phys.* **1984**, *80*, 1976−1981. Schlegel, H. B. *J. Comput. Chem.* **1982**, *3*, 214−218.

(25) Parr, R. G.; Yang, W. *Density Functional Theory of Atoms and Molecules*: Oxford University Press: New York, 1989; Chapter 3.

(26) Jensen, F. *Introduction to Computational Chemistry*; John Wiley & Sons: New York, 1999, Chapter 6.

(27) (a) Hehre, W. J.; Ditchfield, R.; Pople, J. A. *J. Chem. Phys.* **1972**, *56*, 2257−2261. Hariharan, P. C.; Pople, J. A. *Theor. Chim. Acta* **1973**, *28*, 213−222. (b) Frisch, M. J.; Pople, J. A.; Binkley, J. S. *J. Chem. Phys.* **1984**, *80*, 3265−3269. (c) Gordon, M. S.; Binkley, J. S.; Pople, J. A.; Pietro, W. J.; Hehre, W. J. *J. Am. Chem. Soc.* **1982**, 104, 2797. Pietro, W. J.; Francl, M. M.; Hehre, W. J.; Defrees, D. J.; Pople, J. A.; Binkley, J. S. *J. Am. Chem. Soc.* **1982**, 104, 5039. The 6-21G basis set is preferable to the most popular 6-31G basis set in periodic LCAO calculations. To avoid numerical consequences of a badly defined exchange potential or the quasilinear dependence of basis functions, especially for nearly conductive materials such as graphite, the value of the external valence coefficient of carbon is increased from 0.197 to 0.240. This modification would be dangerous for the 6-31G basis set, where the three sp exponential coefficients of the internal valence linear combination are 7.87, 1.88, and 0.54: the 0.54 and the 0.24 gaussian exponents are too close, and this could lead to numerical instabilities. On the other hand, this problem is absent with the 6-21G basis set, where the exponential coefficients of the two internal valence gaussians are 3.66 and 0.77.

(28) Reaction enthalpies and free energies were computed as outlined, for instance, in: (a) Foresman, J. B.; Frisch, Æ. *Exploring Chemistry with Electronic Structure Methods*; Gaussian, Inc.: Pittsburgh, PA, 1996; pp 166−168. (b) McQuarrie, D. A. *Statistical Thermodynamics*; Harper and Row: New York, 1973; Chapter 8. (c) Hill, T. L. *An introduction to Statistical Thermodynamics*; Dover: New York, 1986; pp 438−444.

(29) Gonzalez, C.; Schlegel, H. B. *J. Chem. Phys.* **1989**, *90*, 2154−2161. Gonzalez, C.; Schlegel, H. B. *J. Phys. Chem.* **1990**, *94*, 5523−5527 and references therein.

(30) Frisch, M. J.; Trucks, G. W.; Schlegel, H. B.; Scuseria, G. E.; Robb, M. A.; Cheeseman, J. R.; Zakrzewski, V. G.; Montgomery, J. A., Jr.; Stratmann, R. E.; Burant, J. C.; Dapprich, S.; Millam, J. M.; Daniels, A. D.; Kudin, K. N.; Strain, M. C.; Farkas, O.; Tomasi, J.; Barone, V.; Cossi, M.; Cammi, R.; Mennucci, B.; Pomelli, C.; Adamo, C.; Clifford, S.; Ochterski, J.; Petersson, G. A; Ayala, P. Y.; Cui, Q.; Morokuma, K.; Malick, D. K.; Rabuck, A. D.; Raghavachari K.; Foresman, J. B.; Cioslowski, J.; Ortiz, J. V.; Stefanov, B. B.; Liu, G.; Liashenko, A.; Piskorz, P.; Komaromi, I.; Gomperts, R.; Martin, R. L.; Fox, D. J.; Keith, T.; Al-Laham, M. A.; Peng, C. Y.; Nanayakkara, A.; Gonzalez, C.; Challacombe, M.; Gill, P. M. W.; Johnson, B.; Chen, W.; Wong, M. W.; Andres, J. L.; Head-Gordon, M.; Replogle, E. S.; Pople, J. A. *Gaussian* 03, revision B.05; Gaussian, Inc.: Pittsburgh, PA, 2003.

(31) Saunders, V. R.; Dovesi, R.; Roetti, C.; Orlando, R; Zicovich-Wilson, C. M.; Harrison, N. M.; Doll, K.; Civalleri, B.; Bush, I. J.; D'Arco, Ph; Llunell, M. *CRYSTAL 2003 User Manual*; Turin University: Turin, Italy, 2003. Saunders, V. R.; Dovesi, R.; Roetti, C.; Causà, M.; Harrison, N. M.; Zicovich-Wilson, C. M.; *CRYSTAL'98. User Manual*; Turin University: Turin, Italy, 1999. Pisani, C.; Dovesi, R.; Roetti, C. *Hartree-Fock ab-initio Treatment of Crystalline Systems*; Lecture Notes in Chemistry; Springer-Verlag, Heidelberg, Germany; 1988; Vol. 48.

(32) Dovesi, R.; Pisani, C.; Roetti, C.; Saunders, V. R. *Phys. Rev. B* **1983**, *28*, 5781−5792.

(33) Causà, M.; Dovesi, R.; Orlando, R.; Pisani, C.; Saunders, V. R. *J. Phys. Chem.* **1988**, *92*, 909−913.

(34) Pisani, C.; Aprà E.; Causà M. *Int. J. Quantum Chem.* **1990**, *38*, 395−417.

(35) Zicovich-Wilson, C. M.; Dovesi, R. *Int. J. Quantum Chem.* **1998**, *67*, 299−309.

(36) Doll, K.; Harrison, N. M.; Saunders, V. R. *Int. J. Quantum Chem.* **2001**, *82*, 1−12. Doll, K. *Comput. Phys. Commun.* **2001**, *137*, 74−82. Civalleri, B.; D'Arco, Ph.; Orlando, R.; Saunders, V. R.; Dovesi, R. *Chem. Phys. Lett.* **2001**, *348*, 131−138.

(37) Reed, A. E.; Weinstock, R. B.; Weinhold, F. *J. Chem. Phys.* **1985**, *83*, 735−746. Reed, A. E.; Weinhold, F. *J. Chem. Phys.* **1983**, *78*, 4066−4073. Foster, J. P.; Weinhold, F. *J. Am. Chem. Soc.* **1980**, *102*, 7211−7218.

(38) Molden: Schaftenaar, G.; Noordik, J. H. *J. Comput.-Aided Mol. Design* **2000**, *14*, 123−134 (http://www.cmbi.ru.nl/molden/molden.html) (accessed Oct 2007). XCrySDen: Kokalj, A. *Comput. Mater. Sci.* **2003**, *28*, 155. Code available from http://www.xcrysden.org/ (accessed Oct 2007).

(39) Salem, L. *Electrons in Chemical Reactions*; John Wiley & Sons: New York, 1982; Chapter 7, §4. Spin density values for all systems studied are reported in the Supporting Information. Spin density values from the Mulliken population analysis are also reported, for the sake of comparison.

(40) Hoffmann, R. *Solids and Surfaces: A Chemist's View of Bonding in Extended Structures*; VCH: New York, 1988.

(41) Smirnov, E. P.; Semichinova, O. K.; Abyzov, A. M.; Uffmann, D. *Carbon* **1997**, *35*, 31−34. Chughtai A. R.; Atteya, M. M. O.; Kim, J.; Konowalchuk, B. K.; Smith D. M. *Carbon* **1998**, *36*, 1573−1589. Chughtai, A. R.; Kim, J. M.; Smith, D. M. *J. Atmos. Chem.* **2002**, *43*, 21−43. Saab, E.; Abi-Aad, E.; Bokova, M. N.; Zhilinskaya, E. A.; Aboukais, A. *Carbon* **2007**, *45*, 561−567.

(42) Smith, M. B.; March, J. *March's Advanced Organic Chemistry. Reactions, Mechanisms, and Structure*; John Wiley & Sons: New York, 2001; Chapter 19, §9.